Nanoscale

Accepted Manuscript

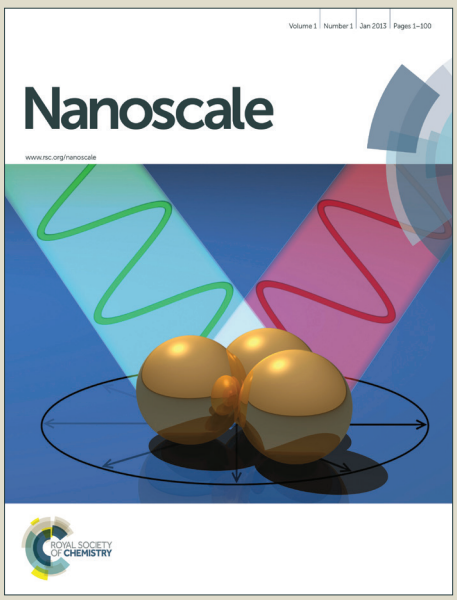

ROYAL SOCIETY OF CHEMISTRY

www.rsc.org/nanoscale

Galactose-functionalized Multi-responsive Nanogels for Hepatoma-targeted Drug Delivery

Shaofeng Lou[1#], Shan Gao[1#], Weiwei Wang[1], Mingming Zhang[1], Ju Zhang[2], Chun Wang[1,3], Chen Li[1*], Deling Kong[1,2], Qiang Zhao[2*]

[1] Tianjin Key Laboratory of Biomaterial Research, Institute of Biomedical Engineering, Chinese Academy of Medical Science, Tianjin 300192, China

[2] State Key Laboratory of Medicinal Chemical Biology, Key Laboratory of Bioactive Materials, Ministry of Education, College of Life Sciences, Nankai University, Tianjin 300071, PR China

[3] Department of Biomedical Engineering, University of Minnesota, Minneapolis, MN 55455, USA.

 # equal contribution

Corresponding authors

Chen Li, PhD

Institute of Biomedical Engineering, BaiDi Road No.236, Tianjin 300192, China

Tel. 0086 22 87893696; Fax 0086 22 87893696

e-mail: cli0616826@gmail.com

Qiang Zhao, PhD

Institute of Molecular Biology, Nankai University, Tianjin 300071, PR China

Tel.: 86-22-23501229; Fax: 86-22-23498775.

E-mail: qiangzhao@nankai.edu.cn

Abstract

We report here a hepatoma-targeting multi-responsive biodegradable crosslinked nanogel, poly(6-O-vinyladipoyl-D-galactose-ss-N-vinylcaprolactam-ss-Methacrylic acid) P(ODGal-VCL-MAA), using a combination of enzymatic transesterification and emulsion copolymerization for intracellular drug delivery. The nanogel exhibited redox, pH and temperature-responsive property, which can be adjusted by varying the monomer feeding ratio. Furthermore, the volume phase transition temperature (VPTT) of the nanogelis was close to body temperature and can result in rapid thermal gelation at 37 °C. Scanning electron microscopy also revealed that the P(ODGal-VCL-MAA) nanogel showed uniform spherical monodispersion. With pyren as a probe, the fluorescence excitation spectra demonstrated nanogel degradation in response to glutathione (GSH). X-ray diffraction (XRD) showed an amorphous property of DOX within the nanogel, which was used in this study as a model anti-cancer drug. Drug-releasing characteristics of the nanogel were examined *in vitro*. The results showed multi-responsiveness of Dox release by variation of environmental pH values, temperature or the availability of GSH, a biological reductase. *In vitro* cytotoxicity assay showed a higher anti-tumor activity of the galactose-functionalized DOX-loaded nanogels against human hepatoma HepG2 cells, which was, at least in part, due to specific binding between the galactose segments and the asialoglycoprotein receptors (ASGP-Rs) in hepatic cells. Confocal laser scanning microscopy (CLSM) and flow cytometric profiles further confirmed elevated cellular uptake of DOX by the galactose-functionalised nanogels. Thus, we report here a multi-responsive P(ODGal-VCL-MAA) nanogel with hepatoma-specific targeting ability for anti-cancer drug delivery.

Keywords: P(ODGal-VCL-MAA); multi-responsive nanogels; glycopolymer; hepatoma-targeting

1. Introduction

Current drug delivery systems is largely dependent on passive diffusion of pharmaceutical compounds from the delivering vehicles.[1-2] Due to the passive diffusion and (EPR) effect, it has been challenging to develop a drug delivery system that could achieve targeted drug delivery and accumulation in tumors.[3-5] Many efforts have been made on the development of stimuli-responsive nanogels for delivery of drug, protein and fluorenscence probe for biomedical applications.[6-12] Nanogel, formed from crosslinked polymeric particles, is a kind of hydrogel with tunable chemical composition and three-dimensional physical structure. Its water content, mechanical properties and biocompatibility could be precisely controlled.[13-15] Nanogels exhibit great potential as delivery vehicles because their flexible size (from nanometers to micrometers) and cross-linked interior network can enhance drug-loading capacity. Their large surface area are suitable for multivalent bioconjugation.[15-17] For delivery of anti-cancer agents, multiple chemical functionalities can be incorporated to the nanogels for targeted and environmental responsive drug delivery.[18-20] Malignant tumors often exhibit distinct characteristics that are different from healthy tissues. As the nanogels delivery system are responsive to the particular environmental factors, including glucose,[20-21] pH,[22-23] temperature,[24-25] presence of redox reactions [26-29] and a complex of multiresponsive,[30-33] this system can minimize the traditional adverse effects of chemotherapy by restricting drug distribution in non-tumor tissues while enhancing drug release and accumulation within tumors. Indeed, previous studies have reported

prolonged systemic circulating period of these stimuli-responsive nanogels and their increased tumor localization through the enhanced permeability and retention (ERP) effect.[13] In addition to the passive EPR effect, active tumor targeting could be achieved by conjugation of bioactive targeting moieties, i.e., carbohydrate moities, [33-37] folic acid, [38] peptide[39] and enzyme[40] to the surface of microgel and nanoparticles.

The asialoglycoprotein receptor (ASGP-R) is one of the most abundantly-expressed receptor in the mammalian hepatocytes. Terminal β-D-galactose (GAL) or N-acetylgalactosamine residues have been recognized as liver-specific targeting ligand for their binding affinity to the ASGP-Rs. Several studies have reported the use of galactosylated polymeric nanoparticles as hepatoma-targeting vehicles for drug, gene delivery and cell surface signal transduction. [22,33-37] Enhanced hepatic uptake was observed after incorporation of galactose residues or lactose moieties to proteins and drug-loaded polymers. Similar results were also shown in nanoparticles and polymeric micelles that have been functionalized with galactose or lactose residues and used as drug delivery carriers for treatment of liver cancer.[41-43]

One limitation of nanogels is their poor biodegradability, which is caused by non-cleavable cross-linkers used for copolymer conjugation. The disulfide bond (-S-S-) is cleavable by endogenous free thiolglutathione (GSH) or metabolic thiols. It has been one of the most commonly used degradable cross-link molecules for the development of anti-cancer drug delivery systems (DDS), and showed excellent biocompatibility and stability within the circulation system.[43-44] The desirable

redox-sensitivity of micelles is verified by changing the concentration of the reducing agent GSH. GSH is an endogenous anti-oxidant that could translocate to the cell surface with an intracellular level within millimolar range (1-10 mM) and extracellular concentration typically at micromolar (20-40 μM) level. [8,27-29,44] Moreover, the intracellular GSH concentration is much higher in cancer cells, which has been an important feature for the development of anti-cancer drug delivery systems.

In the present study, we have designed a multi-responsive and biodegradable nanogel-based drug delivery system with hepatocellular carcinoma targeting property via galactose functionalization. A ligand-directed biodegradable P(ODGal-VCL-MAA) nanogel was prepared. Drug releasing property in response to environmental pH, thermo and redox changes was assessed using DOX as a model anti-cancer drug. Cytotoxicity of the DOX-loaded nanogels was evaluated in human hepatocellular cancer cells (HepG2) and cervical cancer cells (HeLa). Endocytosis of the nanogels and intracellular release of DOX were observed in these two cell lines using confocal microscopy. The up take of DOX by cancer cells was quantified via flow cytometry.

2. Experimental Section

2.1 Materials.

Alkaline protease from Bacillus subtilis (EC 3.4.21.14, a crude preparation of alkaline serine protease, power, 100 U/mg) was purchased from the Wuxi Xue Mei Technological Co. Ltd. N-vinylcaprolactam (VCL, 98% purity), N, N'-bis (acryloyl)

cystamine (BAC), methacrylic acid (MAA) and ammonium persulfate (APS, 98%) were purchased from Sigma Aldrich. Sodium dodecry sulfate (SDS) and galactose were purchased from the Sinopharm Chemical Reagent Co., Ltd. VCL was recrystallized from a n-hexane/toluene mixture. APS was recrystallized from deionized water and dried under vacuum. All solvents were of analytical grade and were dried by storing over activated 4 Å molecular sieves for 24 h prior to use.

2.2 Nanogel preparation

To prepare the galactose-functionalized crosslinked nanogels, polymerizable galactose derivatives, 6-O-vinyladipoyl-D-galactose (ODGal) was synthesized by controllable regioselective enzymatic transesterification of D-galactose and divinyldicarboxylates with alkaline protease as a catalyst in anhydrous pyridine as reported before.[45]

A series of galactose functionalized crosslinked nanogels of poly(6-O-vinyladipoyl-D-galactose-ss-N-vinylcaprolactam-ss-methacrylic acid) P(ODGal-VCL-MAA) were synthesized via free radical precipitation emulsion polymerization. Polymerization was performed in a three-necked flask with condenser attached. Briefly, 1.00 g of VCL and 100 mg MAA, 20.0 mg of SDS, 25.0 mg of $NaHCO_3$, and 40.0 mg of BAC and 58 mg of sodium dodecyl sulfate (SDS) were dissolved in 95 mL of deionized water. The solution was maintained at 70 ^oC under a nitrogen purge and with stirring. After stirring for 30 min, 57 mg of APS was

dissolved in 5 mL of deionized water and injected into the reaction mixture to initiate polymerization. For synthesis of P(ODGal-VCL-MAA) nanogels, VCL, MAA, $NaHCO_3$, SDS, and BAC were dissolved in the reactor at the beginning of the reaction, then a shot of 10.0 mg of ODGal (1 wt % in respect to the sum of MAA and VCL) was added into the reaction mixture after 30 min of polymerization for the formation of ODGal-rich corona. The reaction was maintained under an N_2 atmosphere at 70 ^oC for 6 h. The resulting dispersions were dialyzed (cutoff 8000-14000 Da) against water for 2 weeks to ensure complete removal of unreacted monomers and other small molecules. The synthesis route is depicted in Scheme 1.

Scheme 1. Preparation of galactose-functionalized core crosslinked multi-responsive nanogels and hepatoma-targeting for intracellular release of DOX.

2.3 Characterization

^1H NMR was performed on a Bruker 400 MHz spectrometer using DMSO-d6 as solvent. The degradation of nanogels was determined with a Fluoromax spectrometer (F-7000, Hitachi, Japan) at room temperature. The UV-vis absorption spectra were measured on a UV-vis spectrophotometer (UV-3150, Shimadzu) spectrometer. The average hydrodynamic diameter of the P(ODGal-VCL-MAA) microgels in water were measured by dynamic light scattering (DLS) (Brookhaven BI-200SM goniometer) equipped with a solid state laser source emitting at 532 nm and fitted with an external water bath and thermostat. The volume phase transition temperatures

of the nanogels were examined by microcalorimetric analyses. Known amounts of the dry polymers were equilibrated in distilled water, then 10 mg/mL solutions were studied with a Setaram DSC III instrument. Measurements were performed with a heating rate of 0.5 ℃/min from 0 to 60 °C under a nitrogen atmosphere. The transition temperature was defined as the temperature corresponding to the minimum of the thermogram.[46] Drug loading content (LC) and encapsulation efficiency (EE) were measured with UV-vis spectrophotometer (UV-2550, Shimadzu, Japan). The morphology change of microgels before and after adding 10 mM GSH for 4 h was measured by scanning electron microscope (SEM, JEOL, JSM-7500F).

2.4 DOX-loading and In vitro drug release assay

DOX-loaded nanogels were prepared according to previously reported procedure.[8,14] The dried nanogels (10 mg) were then allowed to stir in water for 24 hours to become fully swollen, and then samples were mixed with different amounts of DOX. The resulting mixtures were stirred for 48 hours, and then centrifuged to precipitate reddish DOX-loaded nanogels.

In vitro drug release experiments were performed as following. 10 mg of freeze-dried DOX-loaded nanogels with 2 mL PBS buffer was placed into a dialysis bag (MWCO 3500). Then the release system was suspended in 10 mL of different temperature, pH buffer solution and aliqout GSH in PBS solution. After a predetermined period, 2 mL of solution was taken from release system for analysis, and 2 mL of fresh medium was added into the release buffer. The DOX concentration of each aliquot was determined by UV-vis analysis at 480 nm. All release experiments

were carried out in triplicate. The release percentage of DOX was calculated using Eq. (1):

$$\text{Drug release } (\%) = \frac{M_t}{M_\infty} \times 100 \quad (1)$$

Where M_t is the amount of DOX released from the nanogels at time t and M_∞ is the amount of the DOX loaded in the nanogels.

2.5 In vitro cytotoxicity assay

Cytotoxicity of DOX-P(VCL-MAA) and DOX-P(ODGal-VCL-MAA) were assessed using a cell counting kit-8 (CCK-8) as previously reported.[47] Briefly, human hepatoma HepG2 and cervical carcinoma HeLa cells were maintained in high-glucose DMEM media (Hyclone) supplemented with 10% fetal bovine serum (FBS), 100 U/mL penicillin and 100 μg/mL under standard cell culture condition (37℃, 5% CO_2/95% air). For both HepG2 and HeLa, the cells were seeded at a density of ~5-6×10^3 cells per well in a 96-well culture plate each. After being in culture overnight, the cells were treated with free DOX, DOX-P(VCL-MAA) and DOX-P(ODGal-VCL-MAA) at a range of designated concentrations for 24 h. The CCK-8 cell viability assay was performed according to the manufacturer's instructions (Dojindo, Japan).

2.6 Cellular uptake of DOX-loaded nanogels

Cellular uptake of DOX-P(VCL-MAA) and DOX-P(ODGal-VCL-MAA) by HeLa and HepG2 cells was examined. Cell were seeded in confocal microscopic

dishes at a density of ~2-3×10^5 cells per dish and cultured overnight. The cells were then exposed to free DOX, DOX-P(VCL-MAA) and DOX-P(ODGal-VCL-MAA) with a final Dox concentration of 5 μg/mL and incubated at 37◦C for 0.5 or 2 h. Then the cells were rinsed with PBS and stained with DAPI (1μg/mL) for 5 min. DOX uptake was examined under a confocal laser scanning microscope (TCS, SP8, Leica, Germany).

To quantify the uptake of Dox by the tumor cells, free DOX, DOX-P(VCL-MAA) and DOX-P(ODGal-VCL-MAA) with a final DOX concentration of 5 μg/mL were incubated with HepG2 or HeLa (~1×10^5) cells for 2 h, following which cellular fluorescent intensity was measured by flow cytometry as previously described.[48] Intracellular DOX level of each sample was presented as average fluorescent intensity.

3 Result and discussion

3.1 Synthesis of the galactose-functionalized crosslinked biodegradable nanogels

P(VCL-MAA) and P(ODGal-VCL-MAA) were first characterized by ^{1}H NMR. As shown in Fig. 1, unambiguous signals were observed at δ=0.8 and 1.3 (CH_2 and CH_3 from MAA and VCL, respectively), δ= 2.0 (CH from MAA), δ=3.5-4.0 (CH_2 on VCL ring), confirming the characteristic structure of P(VCL-MAA). Additional peaks were also detectable at δ=4.5 and δ=6.0 from the P(ODGal-VCL-MAA) nanogel, which confirms the presence of galactose groups.[45,49-50]

Figure 1. ^{1}H NMR spectra of P(VCL-MAA) and P(ODGal-VCL-MAA). ^{1}HNMR was performed on a Bruker 400 MHz spectrometer using DMSO-d_6 as solvent.

SEM images in Fig.2 revealed that the P(VCL-MAA) and P(ODGal-VCL-MAA) nanogels were monodispersed spheres. The size of the microgels increased from 112 ± 3.5 nm to 138 ± 4.1 nm as the molar ratio of ODGal increased from zero to 7.5. It was consistent with the DLS order. The average size of P(VCL-MAA) nanogels was approximately 100-150 nm with a narrow distribution. In contrast, the P(ODGal-VCL-MAA) nanogels were not so uniform in size. It may be due to the presence of the ODGal segment, resulting in an increase in hydrophilicity of the P(ODGal-VCL-MAA) nanogels. In aqueous environment, as the weight fraction of ODGal increased, the growing polymer chains during precipitation polymerization became more hydrophilic. The extended polymer chains failed to undergo efficient chain collapse, leading to a reduced number of particle core and enlarged nanogel size.

Figure 2. SEM images and DLS curves of P(VCL-MAA) (A1, A2), P(ODGal-VCL-MAA) (B1, B2) and DOX-P(ODGal-VCL-MAA) (C1,C2) nanogels in water (1 mg/mL).

3.2 The thermo, pH and redox responsive behavior

Figure 3. Micro-DSC thermograms of PVCL, P(VCL-MAA) and P(ODGal-VCL-MAA) dispersions in aqueous solution.

Phase transitions of the polymeric nanogels were examined by differential scanning calorimetry (DSC). Overall, thermal profile showed a 3 – 5 °C difference between the volume phase transition temperatures of different nanogel compositions, as a result of different relative hydrophilicity of the monomers. Increasing the content of hydrophilic monomer ODGal led to an increase in the VPTT from 32.5 °C with pure VCL to 35.7 and 37.9 °C when the polymers contain 5 and 10 % ODGal. As the ODGal content increases, however, the hydrophilicity of the polymers increases. When the nanogels collapsed, the chains aggregate with one another via a hydrophobic interaction. There is a gain of entropy due to the release of water molecules from around the hydrophobic moieties. This compensates for the loss of entropy arising from the collapse of the polymeric chains resulting in a liquid/solid phase transition. It hence becomes more difficult to compensate for the loss of entropy due to polymer chain collapse, and the VPTT increase. [51,52]

Electrostatic interaction and van der Waal forces could influence the dispersion of nanogels in buffer, which are dependent on surface charge or environmental pH. By changing the pH values, the nanogels could undergo dispersion or aggregation depending on the overall polarity and the surface charges of the nanogels.[30,53] Changes of surface charge of P(VCL-MAA) and P(ODGal-VCL-MAA) at different pH are shown in Table 1. The nanogel composites exhibited only slight negative

surface charge at low pH, which decreased markedly as the pH increased, as a result of deprotonation of the acrylic acid groups.

Table 1: The reproducibility recipes and colloidal details of nanogels

Sample	Feed molar ratio			D_h [b] (nm)/PDI [c]			Zeta potential (mV) [d]			
	VCL	MAA	ODGal	25℃	32℃	37℃	pH 5.0	pH 6.0	pH 7.4	pH 8.0
1	90	10	0	138.4/0.13	112.7/0.11	102.4/0.09	-2.3	-9.6	-13.4	-21.1
2	85	10	5	165.5/0.21	151.7/0.15	133.4/0.11	-1.7	-7.2	-12.2	-19.8
3	85	7.5	7.5	186.9/0.32	177.3/0.23	166.9/0.17	-1.5	-7.0	-10.8	-17.5

a Determined by gravimetric analysis

b Average diameter of nanogels and polydispersity index were determined by DLS at 25 ℃

c The zeta potential of the copolymer solutions was measured by a Zetasizer Nano ZS instrument at room temperature.

To evaluate the reductase (GSH)-triggered degradation of P(ODGal-VCL-MAA), morphological changes of the nanogels in response to GSH was examined. Fig. 4a-c, are the SEM images of P(ODGal-VCL-MAA) nanogels after being exposed to GSH for 0.5 h, 2 h and 4 h. It can be seen that exposure to 10 mM GSH for 4 h resulted in disintegration and shape irregularity of the nanogels. Fluorescence excitation spectra of the P(ODGal-VCL-MAA) nanogels dispersion was also obtained with a pyrene concentration of 6.0×10^{-6} M (Fig. 4d). A sharp decrease of I_{339}/I_{333} can be detected

after addition of 10 mM GSH, indicative of a change of pyrene from hydrophobic to the a polar aqueous property as a result of disulfide bonds cleavage of the copolymer in response to redox changes and subsequent disassembly of the nanogels. [26-29]

Figure 4. SEM graphs achieved after adding 10 mM GSH in nanogels dispersion and incubation with nanogels for 2 h (A), 4 h (B) and after one day (C) in the presence of GSH under ambient conditions.

3.3 The drug loading and releasing property

The X-Ray diffraction of DOX, P(VCL-MAA), P(ODGal-VCL-MAA) and DOX-P(ODGal-VCL-MAA) were shown in the Fig. 5(A). As Eisenberg[54] reported that amorphous or crystalline structure of polymeric capsules play an important role in the loading and release for a drug delivery system, therefore, the crystallinity of samples was investigated with XRD measurement. Broad diffraction peaks were observed in the XRD patterns of P(ODGal-VCL-MAA), indicating that the nanogels were amorphous. In contrast, the XRD patterns of free DOX showed prominent diffraction peaks, suggesting a high crystallinity.[55,56] Importantly, after DOX was loaded into P(ODGal-VCL-MAA), the diffraction peaks and absence of DOX intensity indicated that DOX was either molecularly dispersed or distributed in an amorphous state when encapsulated into microspheres in P(ODGal-VCL-MAA).

Figure 5. (A) XRD spectra of DOX, P(VCL-MAA), P(ODGal-VCL-MAA) and

DOX-P(ODGal-VCL-MAA); (B) In vitro release profiles of DOX from the drug-loaded nanogels under different conditions.

Drug releasing behavior of P(ODGal-VCL-MAA) in response to different stimuli was investigated and the results are shown in Fig. 5 (B).

DOX release from the P(ODGal-VCL-MAA) nanogel in response to different pH was investigated. Since the physiological pH of late endosome, tumor extracellular microenvironment, and normal tissue are 6.0, 6.5 and 7.4, respectively, the DOX-releasing profiles were first assessed at these pH values. It was shown that the DOX release rate increased as the pH decreased from 7.4 to 6.0. This pH-dependent drug releasing property was likely due to the decreased interaction between the MAA segment and DOX upon coinstantaneous protonation of the carboxyl groups and DOX at lower pH. DOX release was the slowest from the P(ODGal-VCL-MAA), which was perhaps due to the electrostatic attraction and hydrophobic interaction between the nanogels and DOX. Drug releasing properties in response to environmental redox changes were also investigated in parallel to assess whether the galactose-functionalized nanogel could be degraded by reductase such as GSH. The release rate of Dox was significantly enhanced in the presence of 10 mM GSH regardless of environmental pH conditions, showing a maximum of 93% drug release within 12 h.

Table 2: Drug loading and antitumor activity of P(VCL-MAA) and P(ODGal-VCL-MAA) nanogels.

Sample	Entrapment efficiency (EE)	Loading content (LC)	IC50(HepG2)	IC50(Hela)
Free DOX	-	-	0.41 μg/mL	0.49 μg/mL
P(VCL-MAA)	76.4%	10.7%	3.04 μg/mL	2.89 μg/mL
P(ODGal-VCL-MAA)	72.85	9.4%	0.63 μg/mL	2.76 μg/mL

The entrapment efficiency (EE) and drug loading (DL) are defined as follows.

$$EE = \frac{\text{Mass of drug loaded in the nanogels}}{\text{Mass of drug feeded initially}} \times 100\%$$

$$LC = \frac{\text{Mass of drug loaded in the nanogels}}{\text{Mass of drug loaded nanogels}} \times 100\%$$

3.4 Assessment of hepatic targeting property and anti-tumor activity

To evaluate the hepatic targeting property of the nanogel-based delivery system and its cytotoxicity, human hepatoma HepG2 cells were used since the galactose groups are expected to recognize the ASGP-R that is overexpressed by HepG2. Human cervical carcinoma cells, Hela which does not express ASGP-R were used as negative control. The Cytotoxicity of Dox-loaded P(VCL-MAA) and P(ODGal-VCL-MAA) was measured by CCK-8 assay. HeLa and HepG2 cells were treated with free DOX or DOX-loaded nanogels at a series of DOX concentrations ranging from 0.01 to 10.0 μg/mL for 24 h. As shown in Fig. 7 and Table 2, the viability of tumor cell was dose-dependent. DOX-loaded P(ODGal-VCL-MAA) nanogels exhibited the highest cytotoxicity in HepG2 cells in comparison to DOX-loaded P(VCL-MAA), which is lack of the liver-targeting galactose groups. Indeed, the half-maximal inhibitory concentration (IC_{50}) values of free DOX, DOX-P(VCL-MAA) and DOX-P(ODGal-VCL-MAA) for HepG2 cells were 0.41,

3.04, and 0.63 μg/mL, respectively. Lower IC_{50} value suggests stronger cytotoxicity of the galactose-functionalized DOX-P(ODGal-VCL-MAA), in comparison to DOX-P(VCL-MAA) which is lack of galactose groups. It is noteworthy that the IC_{50} of DOX-P(ODGal-VCL-MAA) was close to that of free DOX, suggesting excellent drug release and liver-specific targeting. Since hepatocytes could recognize galactose conjugates terminated glycopolymers via receptor-mediated endocytosis, the increased cytotoxicity was expected as a result of ligand receptor-mediated recognition between the ODGal group and ASGP-R on the surface HepG2 cells. Furthermore, the hepatic-specific targeting property of the P(ODGal-VCL-MAA) was confirmed by results obtained from HeLa cells. The IC_{50} of free DOX, DOX-P(ODGal-VCL-MAA) and DOX-P(VCL-MAA) for HeLa cells were at 0.49, 2.89, and 2.76 μg/mL, respectively, suggesting no preference in selectivity between the galactose functionalized P(ODGal-VCL-MAA) and P(VCL-MAA) for Hela cells.

Figure 6. The viability of HepG2 (A1, A2) and Hela (B1, B2) cells at 24 h after incubation with free DOX, DOX-P(ODGal-VCL-MAA) and DOX-P(VCL-MAA) at DOX concentrations ranging from 0.01 to 10 μg/mL. Flow cytometric profiles of HepG2 (A3) and Hela (B3) cells incubated with free DOX (a) DOX-P(VCL-MAA) (b) and DOX-P(ODGal-VCL-MAA) (c) at 37 °C for 2 h. Cells incubated with PBS buffer were used as control.

The cellular uptake of DOX by HepG2 and HeLa cells was quantified by flow

cytometry. As shown in Fig.6 A3 and B3, DOX uptake by HepG2 cells was much higher in the DOX-P(ODGal-VCL-MAA) group than that of DOX-P(VCL-MAA) group. This was not observed in Hela cells, suggesting the selectivity preference of hepatocytes for P(ODGal-VCL-MAA) nanogels as the result of galactose modification.

Figure 7. CLSM images of HepG2 cells incubated with free DOX, DOX-P(VCL-MAA) and DOX-P(ODGal-VCL-MAA) (5 μg/mL) for 0.5 h (a) and 2 h (b). For each panel, the images from right to left show DOX fluorescence in cells (red), cell nuclei stained by DAPI (blue) and overlays of the two images.

Figure 8. CLSM images of Hela cells incubated with free DOX, DOX-P(VCL-MAA) and DOX-P(ODGal-VCL-MAA) (5 μg/mL) for 0.5 h (a) and 2 h (b). For each panel, the images from right to left show DOX fluorescence in cells (red), cell nuclei stained by DAPI (blue) and overlays of the two images.

CLSM was employed to examine the intracellular distribution of DOX after HepG2 and Hela were incubated with free DOX, DOX-P(VCL-MAA) or DOX-P(ODGal-VCL-MAA) nanogels for 0.5 h and 2.0 h. At 0.5 h, DOX (shown as red fluorescence) was mainly observed in the cell cytoplasm in both HepG2 and Hela cells (Fig. 8a,9a). However, at 2 h, DOX was mainly detected within the cell nuclei (Fig. 8b,9b). In addition, morphological changes of membrane diffusion and nuclear

shrinkage were only observed in HepG2 cells treated with DOX-P(OGla-VCL-MAA) for 2 h, not in HeLa cells, again confirming the liver-specific targeting property of P(OGla-VCL-MAA) nanogels.

According to a previous report by Zhong[43] *et al*, disulfide crosslinked glyco-nanoparticles were efficiently taken up by HepG2 cells via a galactose and asialoglycoprotein receptor (ASGP-R) receptor-mediated endocytosis mechanism, in which DOX was released into the nuclei within 4 h. Zhou[30] *et al* found that due to the rapid release of Cur triggered by the high concentration of GSH in tumor cells, as the incubation period of HeLa cells with curcumin-loaded ether anhydride copolymer (mPEG-ss-CPP-SA) micelles was elongated to 3 h, the cells exhibited obvious morphological changes with cell rounding, chromatin condensation and nuclear shrinkage compared with the 0.5 h incubation. Both Yang[8] and Jen[57] prepared multi-responsive microgels and micelles which possessed pH-sensitive comonomers and thus DOX-loaded nanocarriers formed from these polymers were stable at blood pH (7.4) and showed rapid drug release in an acid environment, resulting effective inhibition of the growth of tumor cells due to the increased commulation of therapeutic agent in tumor microenvironment. Combined with polymer multiresponsive and asialoglycoprotein receptor (ASGP-R) targeting properties in our work, we found that our nanogels could enhance the specific binding to liver cancer cells and rapidly deliver DOX to the HepG2 cell nuclei after incubation for 2 h.

Conclusion

In the present study, we prepared a multi-responsive P(ODGal-VCL-MAA) polymeric nanogel with hepatoma-targeting ability for anti-cancer drug delivery. The DOX-loaded nanogels exhibited thermo, pH and GSH-responsive properties. The results of cytotoxicity, CLMS and flow cytometry revealed that P(ODGal-VCL-MAA) nanogels markedly enhanced DOX delivery and inhibition in human hepatoma HepG2 cells as the result of galactose-specific receptor-mediated endocytosis. Thus, our galactose-functionalized multi-responsive nanogels could be potentially used for drug delivery against hepatic cancers.

Acknowledgement

This study was financially supported by National Natural Science Foundation of China (81301309, 51203190 and 51373199), and Chinese Postdoctoral Science Foundation (2013M540062).

References

1. L.A. Lyon, Z. Meng, N. Singh, C.D. Sorrella, A.S. Johna, *Chem. Soc. Rev.,* 2009,38, 865-874.
2. Y. Zhang, H.F. Chan, K.W. Leong, *Adv. Drug Deliv. Rev.* 2013,65, 104–120.
3. L.L. Kiessling, J.C. Grim, *Chem. Soc. Rev.,* 2013,42, 4476-4491.
4. Y. Li, G. H. Gao, D. S. Lee, *Adv. Healthcare Mater.* 2013, 2, 388–417.
5. D. Peer, J. Karp, S. Hong, O. Farokhzad, R. Margalit, R. Langer, *Nature*

Nanotechnol., 2007, 2, 751-760.

6. J. Ramos, A. Imaz, J. E. Forcada, *Polym. Chem.* 2012,3,852-856.
7. K.S. Soppimath, C.W. Tan, Y.Y. Yang, *Adv. Mater*., 2005, 17, 318–323.
8. Y. Wang, J. Nie, B. Chang, Y. Sun, W. Yang, *Biomacromolecules*, 2013,14(9), 3034–3046
9. J. Ding, X. Zhuang, C. Xiao, Y. Cheng, L. Zhao, C. He, Z. Tang, X. Chen, *J. Mater. Chem.*, 2011,21,11383-11391
10. Z. Yu, J.T. Sun, C.Y. Pan, C.Y. Hong, *Chem. Commun.*, 2012,48, 5623-5625
11. S. Zhou, X. Min, H. Dou, K. Sun, C.Y. Chen, C.T. Chen, Z. Zhang, Y. Jin, Z. Shen, *Chem. Commun.*, 2013,49, 9473-9475
12. H. Wang, J. Yi, S. Mukherjee, P. Banerjee, S. Zhou, *Nanoscale,* 2014,6, 13001-13011
13. A.V. Kabanov, S.V. Vinogradov, *Angew. Chem. Int. Ed.*, 2009, 48 , 5418 – 5429
14. J. K. Oh, D.J. Siegwart, H. Lee, G. Sherwood, L. Peteanu, J.O. Hollinger, K. Kataoka, K. Matyjaszewski, *J. Am. Chem. Soc.*2007,129, 5939-5945.
15. L. Li, K. Raghupathi, C. Yuan, S. Thayumanavan, *Chem. Sci.*, 2013,4, 3654-3660
16. D. Sivakumaran, D. Maitland, T. Oszustowicz, T. Hoare, *J. Colloid Interface Sci.,* 2013, 392, 422–430
17. R.K. Shah, J.W. Kim, D.A. Weitz, *Langmuir,* 2010, 26, 1561–1565.
18. Z. Li and T. Ngai, *Nanoscale*, 2013, 5, 1399–1410
19. J. Nicolas, S. Mura, D. Brambilla, N. Mackiewicz, P. Couvreur, *Chem. Soc. Rev.*, 2013, 42, 1147-1235

20. R. Tong, L. Tang, L. Ma, C. Tu, R. Baumgartner, J. Cheng, *Chem. Soc. Rev.*, 2014, 43, 6982-7012

21. T. Ye, S. Yan, Y. Hu, L. Ding, W. Wu, *Polym. Chem.*, 2014,5, 186-194

22. X. Zhang, S. Lu, C. Gao, C. Chen, X. Zhang, M. Liu, *Nanoscale*, 2013, 5, 6498–6506

23. C. Duan, J. Gao, D. Zhang, L. Jia, Y. Liu, D. Zheng, G. Liu, X. Tian, F. Wang, Q. Zhang, *Biomacromolecules,* 2011, 12, 4335–4343.

24. X. Guo, C. Shi, J. Wang, S. Di, S. Zhou, *Biomaterials*, 2013, 34 4544-4554

25. G. Pan, Q. Guo, C. Cao, H. Yang, B. Li, *Soft Matter*, 2013,9, 3840-3850.

26. H. Cai, P. Yao, *Nanoscale*, 2013,5, 2892-2900.

27. Y. Pan, Y. Chen, D. Wang, C. Wei, J. Guo, D.R. Lu, C.C. Chu, C.C. Wang *Biomaterials*, 2012, 33 6570-6579

28. Y.Y. Yang, X. Wang, Y. Hu, H. Hu, D.C. Wu, F.J. Xu, ACS Appl. Mater. Interfaces, 2014, 6, 1044-1052.

29. Q.L. Hua, Q.Y. Jianga, X. Jin, J. Shen, K. Wang, Y.B. Li , F.J. Xu, G.P. Tang, Z.H. Li, Biomaterials 2013, 34, 2265-2276.

30. J. Wang , G. Yang, X. Guo, Z. Tang, Z. Zhong, S. Zhou, *Biomaterials*, 2014, 35, 3080-3090

31. T. Qi, J. Liao, M. Fan, F. Luo, H. Li, Z. Qian, *Nanoscale*, 2012,4, 2694-2704

32. A. R. Maity, A. Chakraborty, A. Mondal, N.R. Jana, *Nanoscale*, 2014,6, 2752-2758

33. S. Bhattacharya, F. Eckert, V. Boyko, A. Pich, *Small*, 2007, 3, 650-657

34. G. Chen, S. Amajjahe, M. H. Stenzel, *Chem. Commun.*, 2009, 1198–1200

35. D.Q. Wu, B. Lu, C. Chang, C.S. Chen, T. Wang, Y.Y. Zhang, S.X. Cheng, X. J. Jiang, X.Z. Zhang, R.X. Zhuo, *Biomaterials*, 2009, 30 1363–1371

36. Y. Zhong, W. Yang, H. Sun, R. Cheng, F. Meng, C. Deng, Z. Zhong, *Biomacromolecules*, 2013, 14, 3723-3730

37. X. Cai, X. Li, Y. Liu, G. Wu, Y. Zhao, F. Chen, Z. Gu, *Pharm. Res.*, 2012 29, 2167–2179.

38. H.X. Wang, M.H. Xiong, Y.C. Wang, J. Zhu, J. Wang, *J. Controlled Release*, 2013, 166,106–114

39. N.V. Nukolova, H.S. Oberoi, S.M. Cohen, A.V. Kabanov, T. K. Bronich *Biomaterials*, 2011, 32, 5417-5426

40. S. S. Dharap, Y. Wang, P. Chandna, J. J. Khandare, B. Qiu, S. Gunaseelan, P. J. Sinko, S. Stein, A. Farmanfarmaian, T. Minko, *Proc. Natl. Acad. Sci. U. S. A.*, 2005 102, 12962–12967.

41. K. C. Wood, N. S. Zacharia, D. J. Schmidt, S. N. Wrightman, B. J. Andaya and P. T. Hammond, *Proc. Natl. Acad. Sci.U. S. A.*, 2008, 105, 2280-2285.

42. J. Ding, C. Xiao, Y. Li, Y. Cheng, N. Wang, C. He, X. Zhuang, X. Zhu, X. Chen, *J. Controlled Release,* 2013, 169 193–203.

43. W. Chen, Y. Zou, F. Meng, R. Cheng, C. Deng, J. Feijen, Z. Zhong, *Biomacromolecules*, 2014, 15, 900-907.

44. J. Liu, W. Huang, Y. Pang, P. Huang, X. Zhu, Y. Zhou, D. Yan, *Angew. Chem. Int. Ed.* 2011, 50, 9162-9166.

45. J. Dai, S. Lin, D. Cheng, S. Zou, X. Shuai, *Angew. Chem. Int. Ed.,* 2011, 50, 9404-9408

46. X. Li, Q. Wu, M. Lu, F. Zhang, X.F. Lin, *J. Polym. Sci. Part A: Polym. Chem.* ,2008,46, 2734–2744.

47. H.G. Schild, M. Muthukumar, D.A. Tirrell, *Macromolecules*, 1991, 24 948–952.

48. W. Wang, C. Li, J. Zhang, A. Dong, D. Kong, *J. Mater. Chem. B*, 2014, 2, 1891–1901

49. P. Huang, H.Song, W. Wang, Y. Sun, J. Zhou, X. Wang, J. Liu, J. Liu, D. Kong, A. Dong, *Biomacromolecules,* 2014, 15, 3128−3138

50. Moshaverinia, A.; Roohpour, N.;Darr, J.A.;Rehman, I.U. *Acta Biomater.,* 2009, 5, 2101–2108.

51. Prabaharan, M.; Grailer, J.J.; Steeber, D.A.; Gong, S. *Macromol. Biosci*. 2008, 8 , 843–851.

52. J. Xu, J. Ye, S. Liu, *Macromolecules,* 2007, 40 9103-9110.

53. L. Li, H. Shan, C. Y. Yue, Y. C. Lam, K. C. Tam, X. Hu, *Langmuir,* 2002, 187291-7298.

54. P. L. Soo, L. Luo, D. Maysinger, A. Eisenberg, *Langmuir,* 2002, 18, 9996−10004

55. X. Jiang, G. Lu, C. Feng, Y. Li, X. Huang, *Polym. Chem.,* 2013, 4, 3876–3884

56. Z. Chen, W. Liu, D. Liu, Y. Xiao, H. Chen, J. Chen, W. Li, H. Cai, W. Li, B. Cai, J. Pan, *J. Controll. Release*, 2012 162, 628–635

57. C.Y. Chen, T.H. Kim, W.C. Wu, C.M. Huang, H.Wei, C.W. Mount, Y. Tian, S.H. Jang, S.H. Pun, A.K. Y. Jen, Biomaterials, 2013, 34 4501-4509.

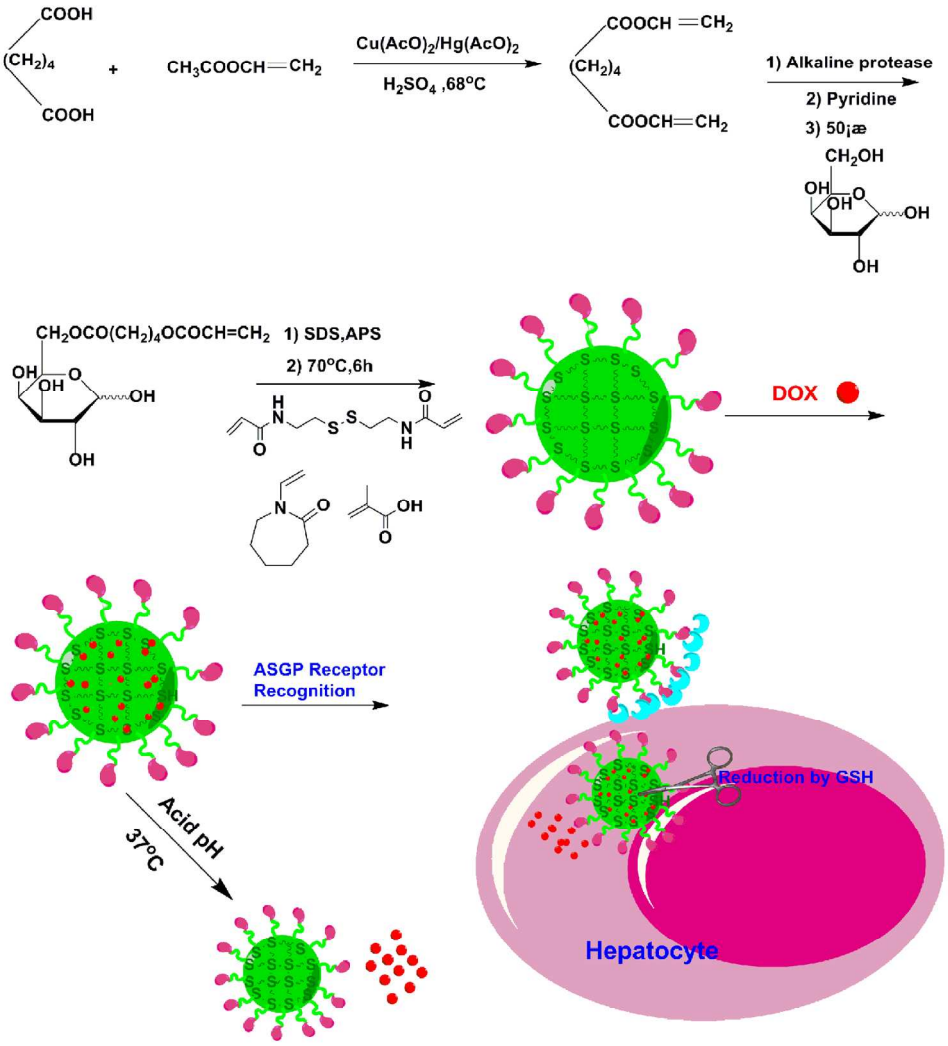

150x186mm (300 x 300 DPI)

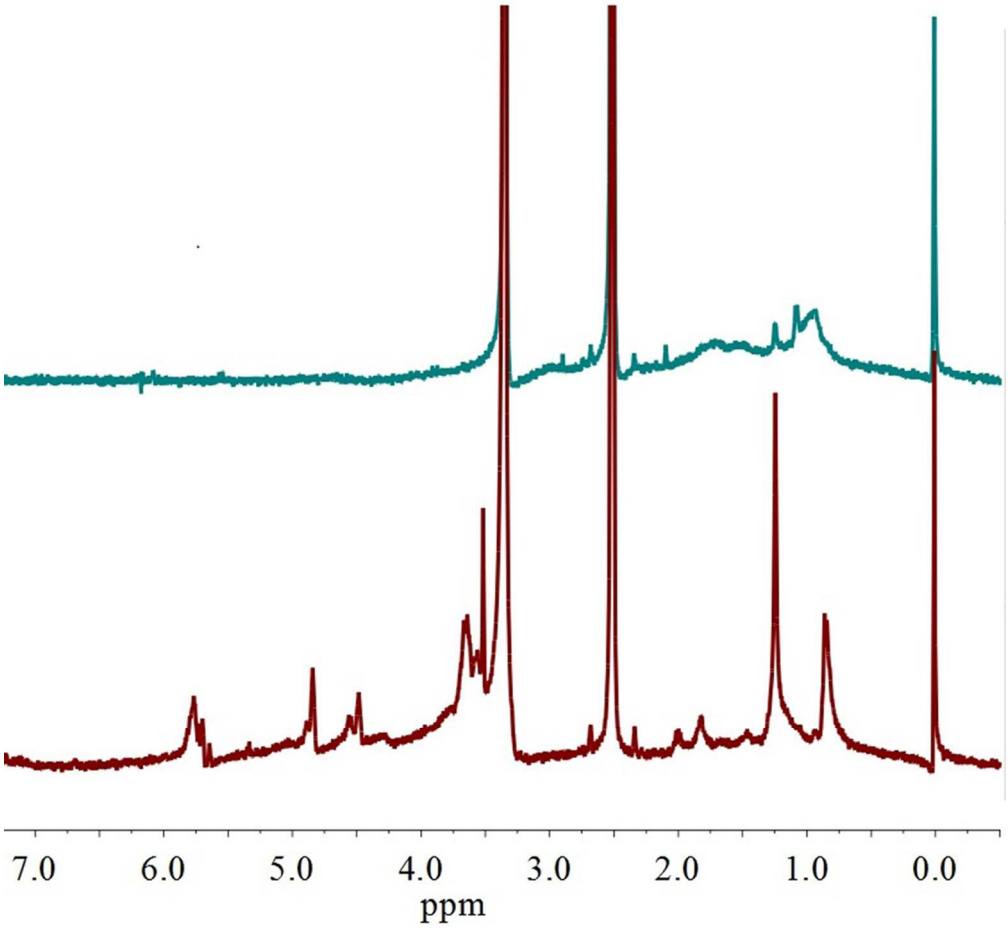

99x93mm (300 x 300 DPI)

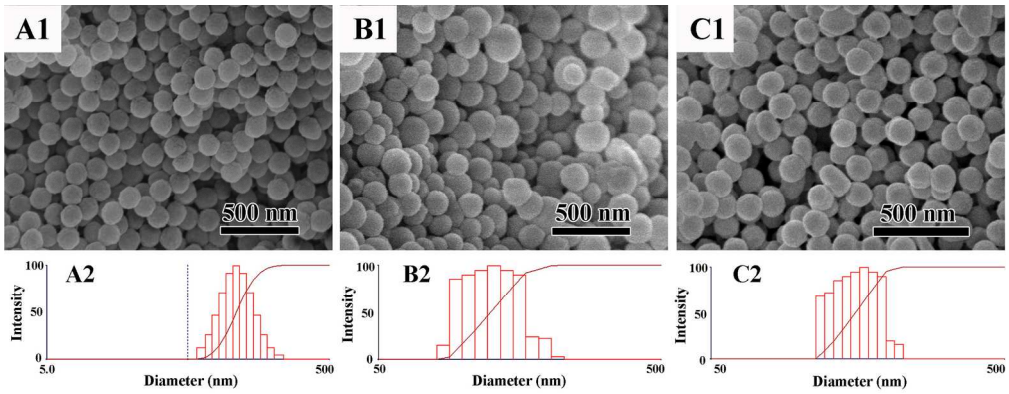

199x77mm (300 x 300 DPI)

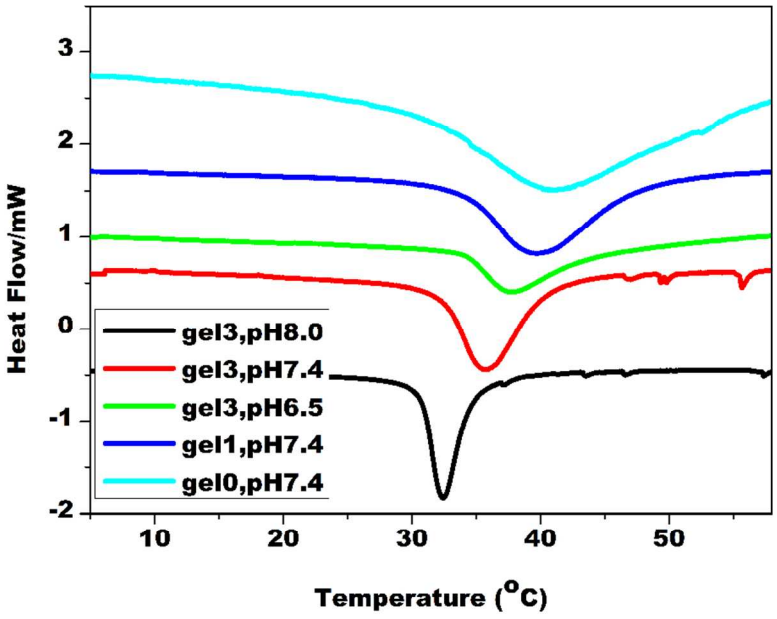

99x70mm (300 x 300 DPI)

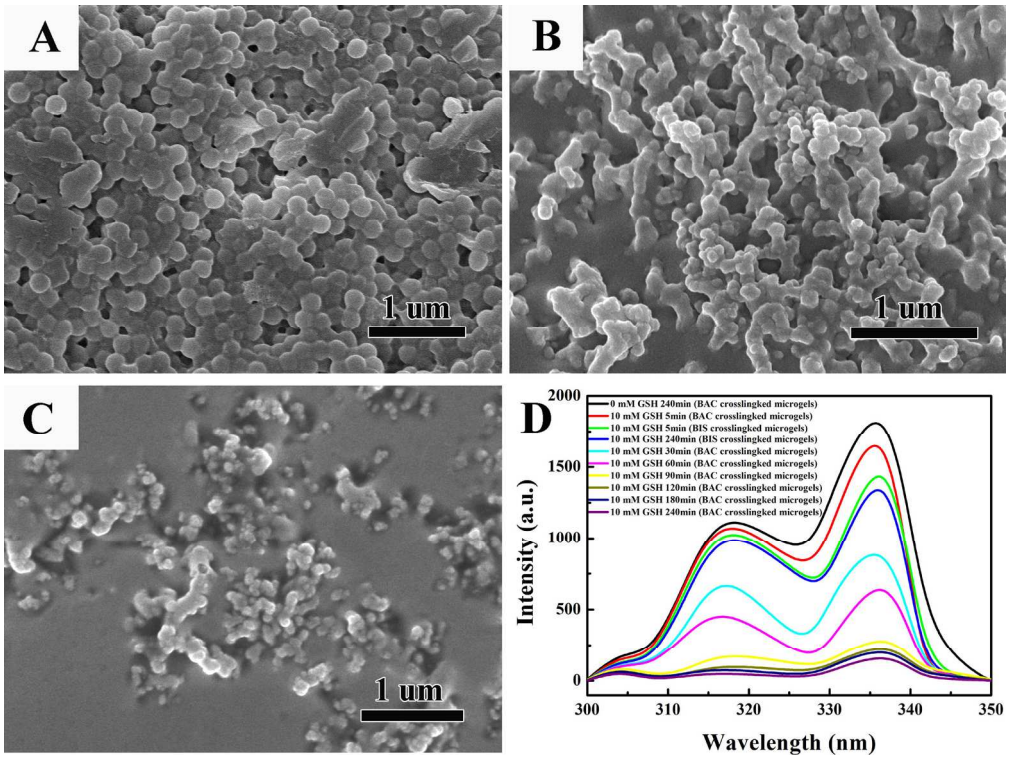

199x149mm (300 x 300 DPI)

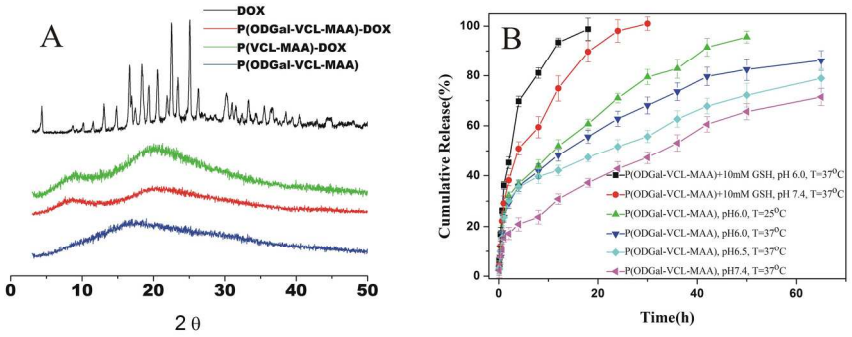

199x74mm (300 x 300 DPI)

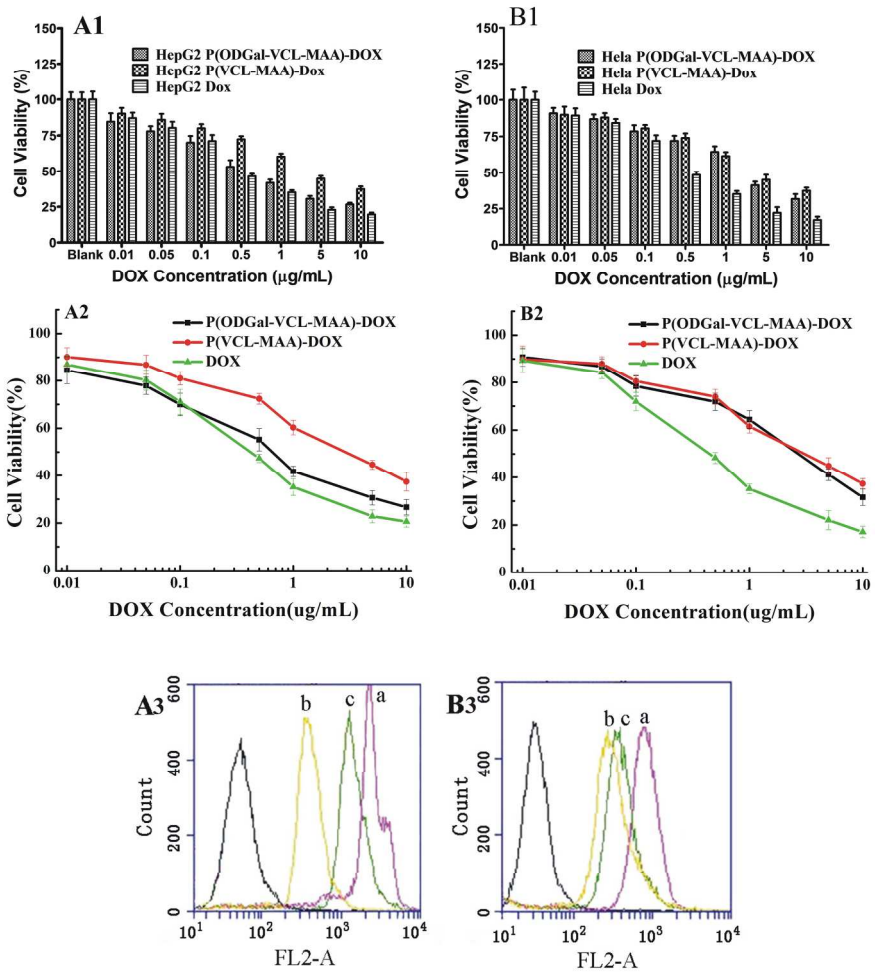

199x199mm (300 x 300 DPI)

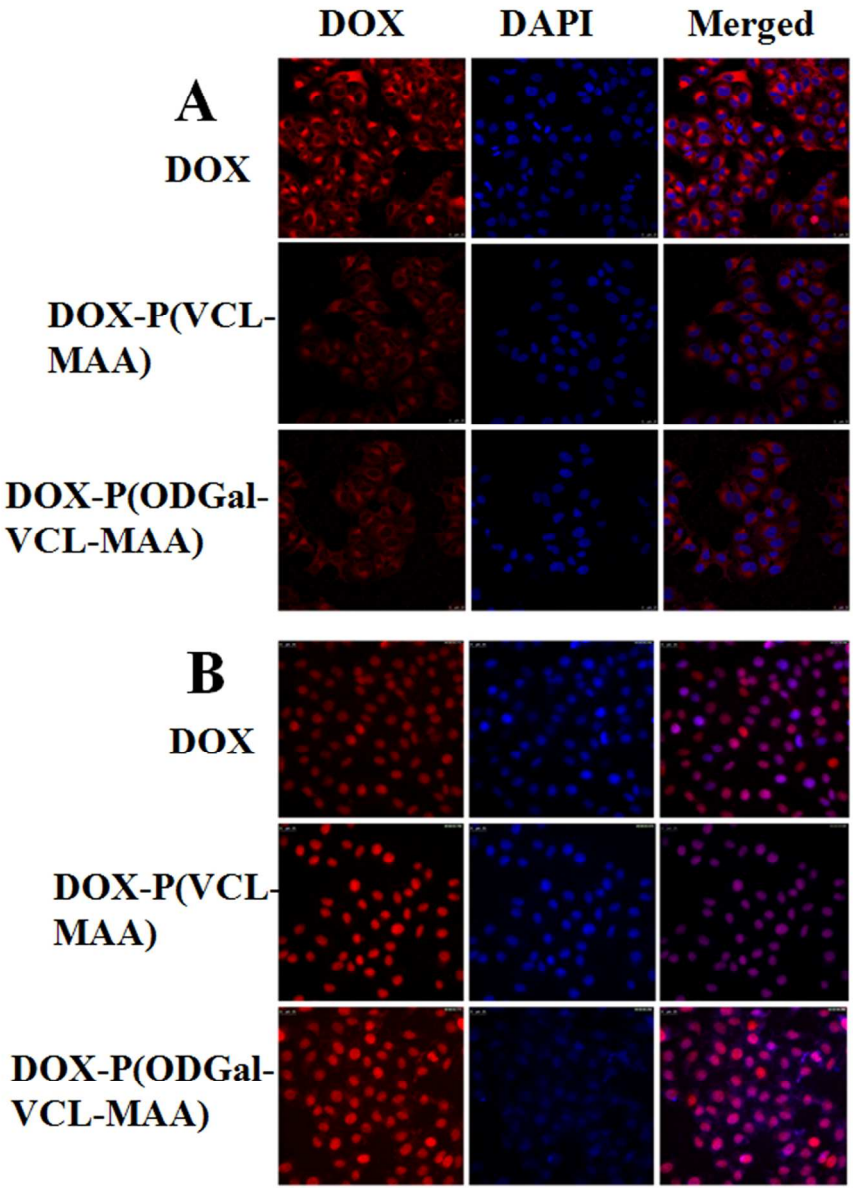

99x126mm (300 x 300 DPI)

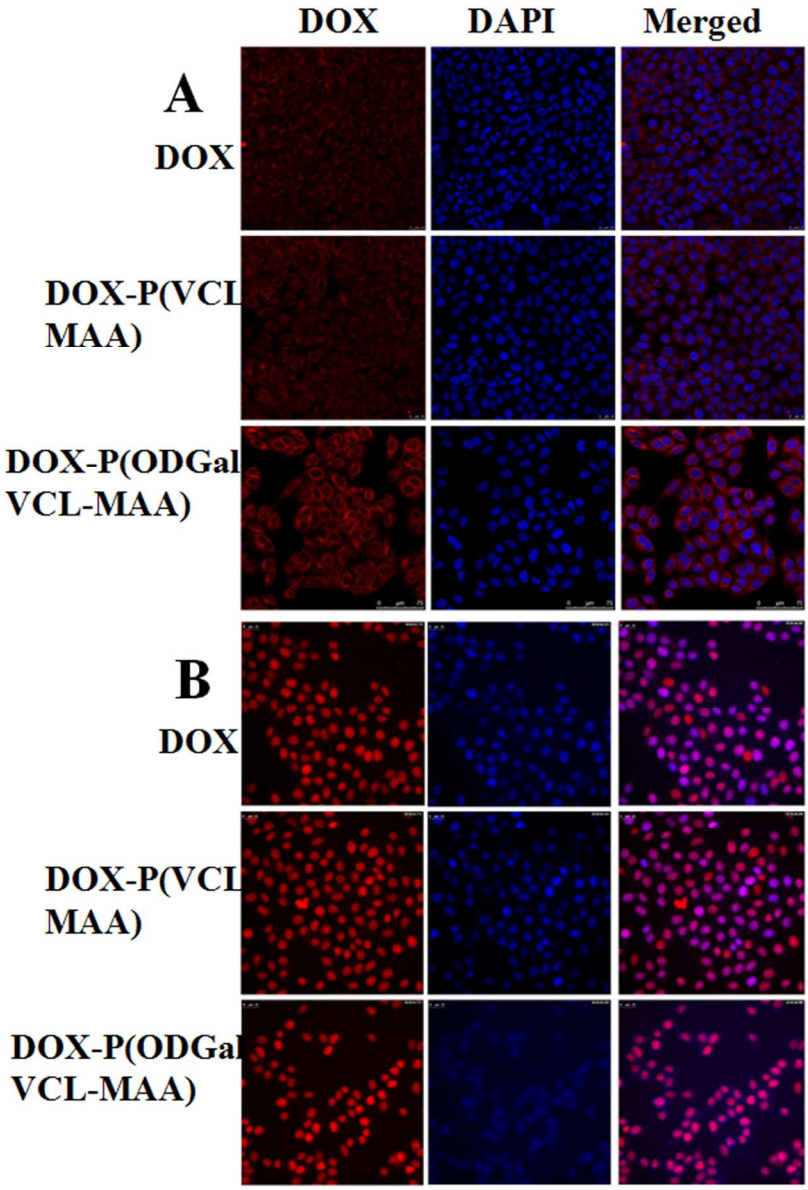

99x135mm (300 x 300 DPI)